Bioorganic & Medicinal Chemistry 21 (2013) 912–921

Contents lists available at SciVerse ScienceDirect

Bioorganic & Medicinal Chemistry

journal homepage: www.elsevier.com/locate/bmc

^{18}F-FBHGal for asialoglycoprotein receptor imaging in a hepatic fibrosis mouse model

Hao-Wen Kao [a,†], Chuan-Lin Chen [a,†], Wen-Yi Chang [a], Jenn-Tzong Chen [b], Wuu-Jyh Lin [b], Ren-Shyan Liu [c,d], Hsin-Ell Wang [a,*]

[a] Department of Biomedical Imaging and Radiological Sciences, National Yang-Ming University, No. 155, Sec. 2, Linong St., Beitou District, Taipei 112, Taiwan, ROC
[b] Department of Isotope Application, Institute of Nuclear Energy Research, Taoyuan, Taiwan, ROC
[c] School of Medicine, National Yang-Ming University, Taipei, Taiwan, ROC
[d] National PET/Cyclotron Center, Veterans General Hospital, Taipei, Taiwan, ROC

ARTICLE INFO

Article history:
Received 28 September 2012
Revised 7 December 2012
Accepted 7 December 2012
Available online 22 December 2012

Keywords:
Liver fibrosis
Asialoglycoprotein receptor
Galactose
MicroPET

ABSTRACT

Quantification of the expression of asialoglycoprotein receptor (ASGPR), which is located on the hepatocyte membrane with high-affinity for galactose residues, can help assess ASGPR-related liver diseases. A hepatic fibrosis mouse model with lower asialoglycoprotein receptor expression was established by dimethylnitrosamine (DMN) administration. This study developed and demonstrated that 4-^{18}F-fluoro-*N*-(6-((3,4,5-trihydroxy-6-(hydroxymethyl)tetrahydro-2*H*-pyran-2-yl)oxy)hexyl)benzamide (^{18}F-FBHGal), a new ^{18}F-labeled monovalent galactose derivative, is an asialoglycoprotein receptor (ASGPR)-specific PET probe in a normal and a hepatic fibrosis mouse models. Immunoassay exhibited a linear correlation between the accumulation of GalH-FITC, a fluorescent surrogate of FBHGal, and the amount of ASGPR. A significant reduction in HepG2 cellular uptake (P <0.0001) was observed using confocal microscopy when co-incubated with 0.5 μM of asialofetuin, a well known ASGPR blocking agent. Animal studies showed the accumulation of ^{18}F-FBHGal in fibrosis liver (14.84 ± 1.10 %ID/g) was appreciably decreased compared with that in normal liver (20.50 ± 1.51 %ID/g, P <0.01) at 30 min post-injection. The receptor indexes (liver/liver-plus-heart ratio at 30 min post-injection) of hepatic fibrosis mice derived from both microPET imaging and biodistribution study were significantly lower (P <0.01) than those of normal mice. The pharmacokinetic parameters ($T_{1/2}\alpha$, $T_{1/2}\beta$, AUC and Cl) derived from microPET images revealed prolonged systemic circulation of ^{18}F-FBHGal in hepatic fibrosis mice compared to that in normal mice. The findings in biological characterizations suggest that ^{18}F-FBHGal is a feasible agent for PET imaging of hepatic fibrosis in mice and may provide new insights into ASGPR-related liver dysfunction.

1. Introduction

The chronic liver disease and cirrhosis, not including hepatoma, were the 8th leading cause of death for men and the 10th for women in Taiwan in 2010.[1] Liver fibrosis is a dynamic and complicatedly regulated wound-healing response, resulting from chronic liver damage due to accumulation of extracellular matrix proteins, which is a characteristic of most types of chronic liver diseases.[2] Hepatitis B and C are the main causes of liver fibrosis. In addition to viral-associated hepatitis, alcohol abuse, non-alcoholic steatohepatitis and autoimmune disease also contribute to the pathogenesis of liver fibrosis.[3] The fibrotic response underlies virtually all the complications of end-stage liver disease, including portal hypertension, ascites, encephalopathy, synthetic dysfunction, and impaired metabolic capacity. Liver fibrosis is reversible,[2,4] whereas advanced cirrhosis may not be completely reversible, and recovery depends on the etiology and stage of the disease. Thus, early detection of liver fibrosis in patients has become an important clinical issue for predicting the prognosis and early treatment to prevent disease progression.

Traditionally, liver biopsy and histological examination is considered the 'gold standard' for identifying the cause of liver disease and assessing the stage of fibrosis. However, several limitations were recognized for this invasive procedure, such as the possibility of sampling error, intra- and inter-observer variation, and only provides a static data.[5] In recent years, several imaging approaches have been adapted to detect liver fibrosis[6] including ultrasonography (FibroScan[7] and acoustic radiation force impulse[8]), CT and MRI. These morphologic imaging techniques mainly provide information about structural aspects of liver fibrosis, such as the

* Corresponding author. Tel.: +886 2 28267215; fax: +886 2 28201095.
E-mail addresses: hewang@ym.edu.tw, hewang2@gmail.com (H.-E. Wang).
† These authors contributed equally to this work.

0968-0896/$ - see front matter © 2012 Elsevier Ltd. All rights reserved.
http://dx.doi.org/10.1016/j.bmc.2012.12.022

changing in liver echogenicity and nodularity, degree of liver stiffness as well as signs of portal hypertension. Molecular imaging is a new biomedical discipline that enables the visualization, characterization, and quantification of biologic processes at the cellular and molecular levels within living subjects. Thus, efforts to diagnose liver fibrosis down to the molecular level using non-invasive strategy have direct clinical implications.

The asialoglycoprotein receptors (ASGPR) are renowned for existing in the mammalian liver and located on the surface of hepatocytes which contain 100,000–500,000 binding sites per cell.[9,10] The receptors play an essential role in maintaining serum glycoprotein homeostasis by the recognition, binding, and endocytosis of glycoprotein owning galactose residues on the terminal position of saccharide chain, such as asialoglycoproteins.[11,12] After internalized via clathrin-coated pits and fused with endosomes, the asialoglycoproteins are released in the acidic environment of the endosome and transported to lysosomes for degradation, while the receptor is recycled back to the cell surface. In the previous reports,[13,14] Sawamura et al. demonstrated that the asialoglycoprotein receptor activity in the cirrhotic liver was about 28% of the control value in patients. Since 1985, ^{99m}Tc-labeled neoglycoalbumin (^{99m}Tc-NGA)[15,16] and ^{99m}Tc-labeled galactosyl-human serum albumin (^{99m}Tc-GSA)[17–19] were developed as single photon emission computed tomography (SPECT) imaging probes for acquiring the asialoglycoprotein receptor scintigraphy to evaluate the liver function. Fluorine-18 labeled galactosyl-neoglycoalbumin (^{18}F-FNGA)[20] was presented as a radiotracer for positron emission tomography (PET) scans. In recent years, polymer backbone radiotracers were also reported as ASGPR targeting agents, such as chitosan[21] and poly(vinylbenzyl-*O*-β-D-galactopyranosyl-D-gluconamide) (PVLA).[22] Although the exact physiological role of ASGPR has not been elucidated, previous studies suggested that an abnormal cell-surface distribution of this receptor might occur in the liver dysfunction such as cirrhosis or liver cancer.[12,23] Evaluation of ASGPR expression based on ^{99m}Tc-NGA scintigraphic imaging has been employed for distinguishing and monitoring the graft and native liver functions in patients.[24]

Although previous studies had suggested that the in vitro ASGPRs binding affinity of multi- and di-valent galactoside were 10^4 to 10^5-fold and 10-fold higher than the monovalent ligand,[25,26] a ^{18}F-labled monoantennary galactoside may still be useful for noninvasive evaluation of ASGPR-related hepatic fibrosis owing to the much rapid pharmacokinetics than that of multivalent macromolecules in vivo. This study reported for the first time a monoantennary galactose derivative 4-^{18}F-fluoro-*N*-(6-((3,4,5-trihydroxy-6-(hydroxymethyl)tetrahydro-2*H*-pyran-2-yl)oxy)hexyl)benzamide (^{18}F-FBHGal) as a ASGPR-specific PET probe. The biological evaluations demonstrate that ^{18}F-FBHGal PET can characterize the reduction of ASGPR in liver fibrosis in a dimethylnitrosamine (DMN)-treated mouse model and may have the potential to evaluate ASGPR-related liver disease.

2. Materials and methods

2.1. Synthesis of β-D-galactosyl precursor for ^{18}F labeling and the authentic standard of FBHGal

The synthetic scheme is shown in Figure 1. Nuclear magnetic resonance (NMR) spectra were recorded on a Bruker Avance III 400 MHz NMR spectrometer or Varian 500 MHz NMR spectrometer and referenced to $CDCl_3$ (^{1}H NMR: $CDCl_3$ at 7.24 ppm and ^{13}C NMR: $CDCl_3$ at 77.0 ppm), DMSO-d_6 (^{1}H NMR: DMSO-d_6 at 2.49 ppm and ^{13}C NMR: DMSO-d_6 at 39.5 ppm) and methanol-d_4 (^{1}H NMR: methanol-d_4 at 3.30 ppm and ^{13}C NMR: methanol-d_4 at 49.0 ppm).

2.1.1. Synthesis of 6-(acetoxymethyl)tetrahydro-2*H*-pyran-2,3,4,5-tetrayl tetraacetate (*1*) (α/β = 1.9)

A mixture of β-D-galactose (2.0 g, 11.1 mmol) and acetic anhydride (10.0 mL, 106.0 mmol) in anhydrous pyridine (14 mL) was stirred at ambient temperature for 24 h. The reaction mixture was quenched by cold water (50 mL) and extracted by ethyl acetate (50 mL × 3), washed with water (20 mL × 3) and brine. The organic layer was dried and evaporated under vacuum to give compound **1** as yellow syrup (4.1 g, 95% yield). R_f = 0.54 (silica gel 60F_{254} on an aluminum sheet, ethyl acetate/hexane = 3/2 as the developing agent). ^{1}H NMR (400 MHz, $CDCl_3$): δ 6.35 (br, 1H, H-1$_\alpha$), 5.68 (d, *J* = 8.2 Hz, 0.5H, H-1$_\beta$), 5.48 (br, 1H, H-4$_\alpha$), 5.40 (d, *J* = 8.2 Hz, 0.5H, H-4$_\beta$), 5.34–5.29 (m, 2.5H, H-2$_\alpha$, H-2$_\beta$, H-3$_\alpha$), 5.05 (dd, *J* = 10.5, 3.4 Hz, 0.5H, H-3$_\beta$), 4.35–4.29 (m, 1.5H, H-6$_\beta$, H-5$_\alpha$), 4.17–4.03 (m, 3.0H, 2 H-6$_\alpha$, H-6$_\beta$, H-5$_\beta$), 2.14 (s, 1.6H, CH_3CO_β), 2.14 (s, 3H, CH_3CO_α), 2.14 (s, 3H, CH_3CO_α), 2.03 (s, 1.6H, CH_3CO_β), 2.02 (s, 3.2H, 2 CH_3CO_β), 2.02 (s, 3H, CH_3CO_α), 2.00 (s, 3H, CH_3CO_α), 1.98 (s, 3H, CH_3CO_α), 1.97 (s, 1.6H, CH_3CO_β).

2.1.2. Synthesis of 2-(acetoxymethyl)-6-bromotetrahydro-2*H*-pyran-3,4,5-triyl triacetate (2)

A mixture of β-D-galactosyl pentaacetate **1** (3.9 g, 10.0 mmol) in an anhydrous methylene chloride (100 mL) was added acetic acid (4 mL), acetic anhydride (4 mL) and hydrobromic acid solution (33% in acetic acid) under 0 °C. The reaction mixture was stirred overnight at ambient temperature, then quenched with cold water and extracted by methylene chloride (50 mL × 3). The organic layer was dried and evaporated under vacuum to give compound **2** as yellow syrup (4.0 g, 98% yield). R_f = 0.61 (silica gel 60F_{254} on an aluminum sheet, ethyl acetate/hexane = 1/2 as the developing agent). ^{1}H NMR (400 MHz, $CDCl_3$): δ 6.67 (d, *J* = 4.0 Hz, 1H, H-1′), 5.49 (d, *J* = 3.2 Hz, 1H, H-4′), 5.38 (dd, *J* = 10.8, 3.2 Hz, 1H, H-3′), 5.02 (dd, *J* = 10.8, 4 Hz, 1H, H-2′), 4.46 (dd, *J* = 6.4, 6.4 Hz, 1H, H-5′), 4.16 (dd, *J* = 11.2, 6.4 Hz, 1H, H-6′), 4.08 (dd, *J* = 11.2, 6.4 Hz, 1H, H-6′), 2.13 (s, 3H, CH_3CO), 2.10 (s, 3H, CH_3CO), 2.03 (s, 3H, CH_3CO), 1.99 (s, 3H, CH_3CO).

2.1.3. Synthesis of 4-fluoro-*N*-(6-hydroxyhexyl)-benzamide (FHB, 3)

6-Aminohexanol (1.0 g, 8.5 mmol), dissolved in dichloromethane (17 mL) containing triethylamine (3.6 mL, 26.0 mmol) was added *p*-fluorobenzoyl chloride (1.0 mL, 8.5 mmol) dropwise at 0 °C. The mixture was stirred overnight at ambient temperature. The crude product was washed with cold pure water (30 mL × 2), dried and evaporated under vacuum. After recrystallized in a mixed solvent of dichloromethane and hexane, the desired compound was obtained as a white crystalline solid (1.8 g, 90% yield). ^{1}H NMR (500 MHz, DMSO-d_6): δ 8.44 (br, 1H, NH), 7.89 (dd, *J* = 8.5 Hz, J_{HF} = 6.0 Hz, 2H, Ar), 7.26 (dd, *J* = 8.5 Hz, J_{HF} = 7.0 Hz, 2H, Ar), 3.38–3.35 (m, 2H, CH_2O), 3.38–3.35 (m, 1H, OH), 3.21 (dt, *J* = 6.5, 6.5 Hz, 2H, NCH_2), 1.51–1.48 (m, 2H, $NCCH_2$), 1.41–1.38 (m, 2H, CH_2CO), 1.30–1.21 (m, 4H, CH_2); ^{13}C NMR (125 MHz, DMSO-d_6): 165.0 (C═O), 163.8 (d, J_{CF} = 246.8 Hz, F-C), 131.2 (Ar), 29.7 (d, J_{CF} = 9.1 Hz, Ar), 115.1 (d, J_{CF} = 21.5 Hz, Ar), 60.6 (CH_2OH), 39.1 ($NHCH_2$), 32.4 (CH_2CH_2OH), 29.1 ($NHCH_2CH_2$), 26.4, 25.2 (CH_2); HRESI-MS: calcd for $C_{13}H_{18}FNNaO_2^+$ 262.1214 (M+Na$^+$), found 262.1205 (M+Na$^+$).

2.1.4. Synthesis of 4-fluoro-*N*-(6-((3,4,5-trihydroxy-6-(hydroxymethyl)tetrahydro-2*H*-pyran-2-yl)oxy)hexyl) benzamide (FBHGal, 4a)

A mixture of compound **2** (500.0 mg, 1.2 mmol), compound **3** (438.0 mg, 1.8 mmol), silver carbonate (330.0 mg, 1.2 mmol), and activated 4 Å molecular sieves (1.0 g) was added in anhydrous dichloromethane (2.5 mL) at 0 °C. After stirring for 24 h under an

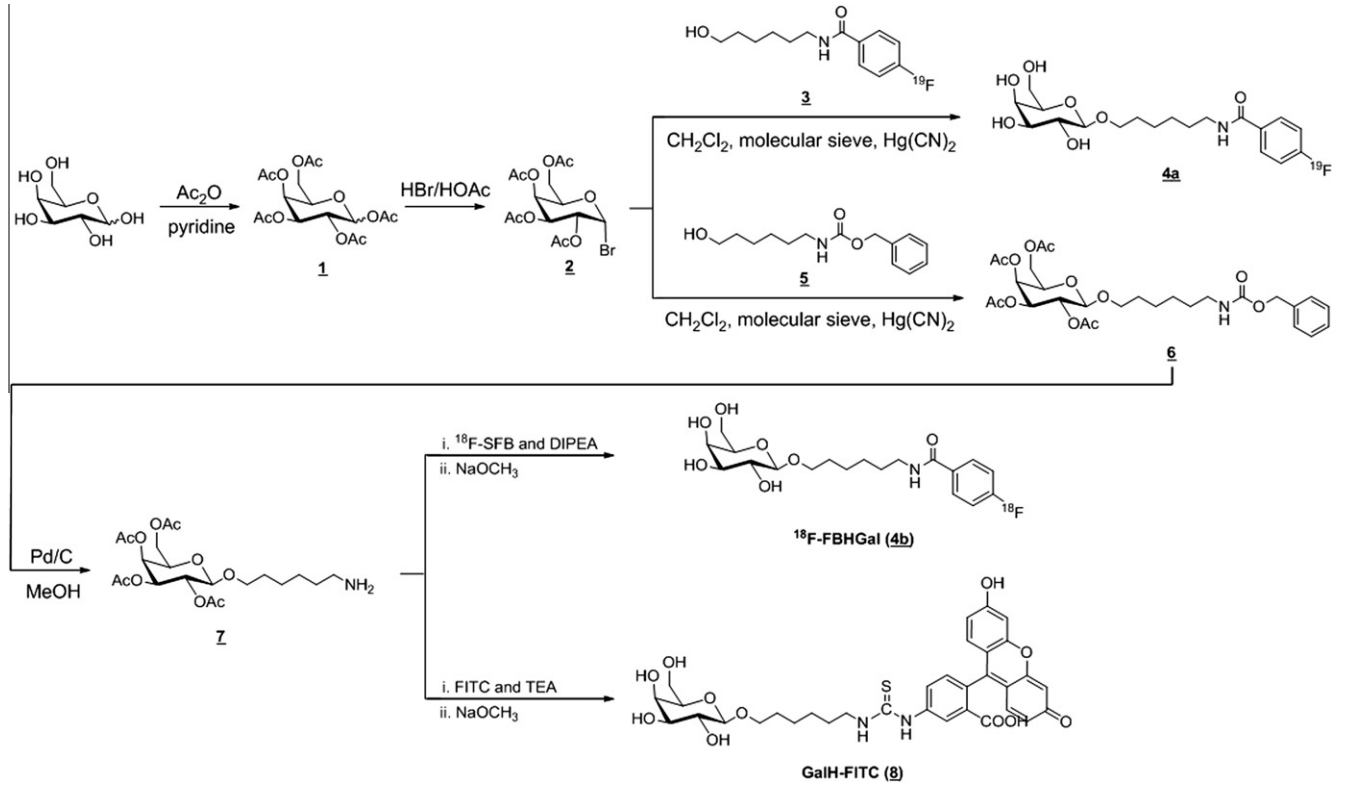

Figure 1. Synthesis of ^{18}F-labeled and FITC-conjugated monomeric galactose derivatives, ^{18}F-FBHGal and GalH-FITC.

argon atmosphere at ambient temperature, the result solution was filtered through celite, and washed with dichloromethane (2 mL). The filtrate was washed with saturated aqueous sodium bicarbonate (30 mL), dried and evaporated under vacuum. The crude products (a mixture of α- and β-galactopyranosides) were purified by flash chromatography (eluent, ethyl acetate/hexane = 1/1). The crude product re-dissolved in anhydrous methanol (1.5 mL) was treated with 0.5 M sodium methoxide in methanol (0.02 mL). After stirring for 24 h, the reaction mixture was filtered through celite and evaporated to give compound **4a** as a white solid (122.4 mg, 25% yield). ^{1}H NMR (500 MHz, methanol-d_4): δ 7.85 (dd, J = 8.0 Hz, $J_{H\text{-}F}$ = 5.6 Hz, 2H, H-10, H-12), 7.17 (dd, J = 8.0 Hz, $J_{H\text{-}F}$ = 8.0 Hz, 2H, H-9, H-13), 4.20 (d, J = 7.0 Hz, 1H, H-1′), 3.89 (dt, J = 9.5, 6.5 Hz, 1H, H-1), 3.83 (d, J = 3.0 Hz, 1H, H-4′), 3.76–3.69 (m, 2H, H-6′), 3.54 (dt, J = 9.5, 6.5 Hz, 1H, H-1), 3.52–3.44 (m, 3H, H-2′, H-3′, H-5′), 3.36 (t, J = 7.0 Hz, 2H, H-6), 1.65–1.60 (m, 4H, H-2, H-5), 1.44–1.40 (m, 4H, H-3, H-4); ^{13}C NMR (125 MHz, methanol-d_4): 168.9 (C, C=O), 166.0 (d, J = 22.0 Hz, C, C-11), 132.1 (C, C-8), 130.8 (d, J = 9.0 Hz, C, C-9, C-13), 116.3 (d, J = 9.0 Hz, C, C-10, C-12), 104.9 (CH, C-1′), 76.5 (CH, C-5′), 75.0 (CH, C-3′), 72.5 (CH, C-2′), 70.6 (CH_2, C-1), 70.2 (CH, C-4′), 62.4 (CH_2, C-6′), 40.9 (CH_2, C-6), 30.6 (CH_2, C-2), 30.3 (CH_2, C-5), 27.8 (CH_2, C-4), 26.7 (CH_2, C-3); HRESI-MS: calcd for $C_{19}H_{28}FNNaO_7^+$ 424.1742 (M+Na$^+$), found 424.1730 (M+Na$^+$).

2.1.5. Synthesis of benzyl-(6-hydroxyhexyl)carbamate (5)

6-aminohexanol (5.0 g, 42.7 mmol) dissolved in a mixture of tetrahydrofuran (50 mL) and water (15 mL) was added benzylchloroformate (7.3 mL, 51.2 mmol) dropwise at 0 °C. Sodium hydroxide (1 N, 12 mL) was added at the same temperature for 30 min to keep the pH of the reaction solution at 8–9 then stirred at ambient temperature for additional 30 min. The reaction mixture was extracted with diethyl ether (30 mL × 3), dried and evaporated under vacuum. After recrystallized in a mixed solvent of dichloromethane and hexane, the desired compound was obtained as a white crystalline solid (3.85 g, 90% yield). ^{1}H NMR (400 MHz, $CDCl_3$): δ 7.34 (m, 5H, Ar), 5.07 (s, 2H, PhCH_2), 4.73 (br, NH), 3.61 (t, J = 6.4 Hz, 2H, CH_2O), 3.16 (dt, J = 6.8, 6.8 Hz, 2H, NCH_2), 1.61–1.32 (m, 8H, CH_2); ^{13}C NMR (100 MHz, $CDCl_3$): 156.4 (C, C=O), 136.6, 128.5, 128.1 (CH, Ar), 66.6 (CH_2, $PhCH_2$), 62.7 (CH, CH_2OH), 40.9 (CH, $NHCH_2$), 32.5 (CH_2, CH_2CH_2OH), 29.9 (CH_2, $NHCH_2CH_2$), 26.3 (CH_2, $CH_2CH_2CH_2OH$), 25.3 (CH_2, $NCH_2CH_2CH_2$).

2.1.6. Synthesis of 2-(acetoxymethyl)-6-((6-(((benzyloxy) carbonyl)amino)hexyl)oxy)tetrahydro-2*H*-pyran-3,4,5-triyl triacetate (6)

Starting from 6-(*N*-benzyloxycarbonylamino)-hexanol, compound **6** was synthesized in 26% yield using a procedure similar to that of compound **4a**. ^{1}H NMR (400 MHz, $CDCl_3$): δ 7.32 (m, 5H, Ar), 5.36 (d, J = 3.6 Hz, 1H, H-4′), 5.17 (dd, J = 10.4, 8.0 Hz, 1H, H-2′), 5.06 (s, 2H, Ar-CH_2), 4.99 (dd, J = 10.6, 3.6 Hz, 1H, H-3′), 4.41 (d, J = 8.0 Hz, 1H, H-1′), 4.16 (dd, J = 11.2, 6.8 Hz, 1H, H-6′), 4.10 (dd, J = 11.2, 6.8 Hz, 1H, H-6′), 3.88–3.83 (m, 2H, H-1, H-5′), 3.43 (dt, J = 9.6, 6.8 Hz, 1H, H-1), 3.16 (dt, J = 13.0, 6.8 Hz, 2H, H-6), 2.13 (s, 3H, CH_3CO), 2.06 (s, 6H, CH_3CO), 1.95 (s, 3H, CH_3CO), 1.54–1.28 (m, 8H, H-2, H-3, H-4, H-5); ^{13}C NMR (100 MHz, $CDCl_3$): 170.3, 170.2, 170.1, 169.3, 156.3 (C, C=O), 136.6 (C, C-9), 128.4, 128.0 (CH, Ar), 101.2 (CH, C-1′), 70.9 (CH, C-3′), 70.5 (CH, C-5′), 70.0 (CH_2, C-1), 68.8 (CH, C-2′), 67.0 (CH, C-4′), 66.5 (CH_2, C-8), 61.2 (CH_2, C-6′), 40.8 (CH_2, C-6), 29.2, 26.3, 25.4 (CH_2, C-2, C-3, C-4, C-5), 20.7, 20.6, 20.5 (CH_3, CH_3CO); ESI-MS: calcd for $C_{28}H_{39}NNaO_{12}$ 604.2 (M+1), found 604.4 (MH$^+$). HRESI-MS: calcd for $C_{28}H_{39}NNaO_{12}^+$ 604.2364 (M+Na$^+$), found 604.2355 (M+Na$^+$).

2.1.7. Synthesis of 2-(acetoxymethyl)-6-((6-aminohexyl)oxy)-tetrahydro-2*H*-pyran-3,4,5-triyl triacetate (7)

A mixture of above product **6** (200.0 mg, 0.34 mmol) and 10% Pd/C (50 mg) was added in anhydrous methanol (1.7 mL) and stirred under 1 atm of hydrogen for 24 h. The reaction mixture was purged through celite and evaporated under vacuum to give a thick

oil of **7** (150.0 mg, 98% yield). ^{1}H NMR (400 MHz, $CDCl_3$): δ 5.35 (d, J = 3.6 Hz, 1H, H-4′), 5.13 (dd, J = 10.4, 8.0 Hz, 1H, H-2′), 4.99 (dd, J = 10.6, 3.6 Hz, 1H, H-3′), 4.43 (d, J = 8.0 Hz, 1H, H-1′), 4.15 (dd, J = 11.2, 6.4 Hz, 1H, H-6′), 4.08 (dd, J = 11.2, 7.2 Hz, 1H, H-6′), 3.90–3.81 (m, 2H, H-1, H-5′), 3.44 (dt, J = 9.6, 6.8 Hz, 1H, H-1), 2.96 (t, J = 7.6 Hz, 2H, H-6), 2.11 (s, 3H, CH_3CO), 2.06 (s, 3H, CH_3CO), 2.04 (s, 3H, CH_3CO), 1.96 (s, 3H, CH_3CO), 1.61–1.12 (m, 8H, H-2, H-3, H-4, H-5); ^{13}C NMR (100 MHz, $CDCl_3$): 170.4, 170.2, 170.1, 169.6 (C, C═O), 101.2 (CH, C-1′), 71.0 (CH, C-2′), 70.8 (CH, C-5′), 70.5 (CH_2, C-1), 68.9 (CH, C-3′), 66.9 (CH, C-4′), 61.1 (CH_2, C-6′), 39.4 (CH_2, C-6), 29.3, 29.1, 26.5, 25.5 (CH_2, C-2, C-3, C-4, C-5), 20.8, 20.7, 20.6 (CH_3, CH_3CO); ESI-MS: calcd for $C_{20}H_{34}NO_{10}$ 448.2 (M+1), found 448.3 (MH^+).

2.1.8. Synthesis of 2-(6-hydroxy-3-oxo-3*H*-xanthen-9-yl)-5-(3-(6-((-3,4,5-trihydroxy-6-(hydroxymethyl)tetrahydro-2*H*-pyran-2-yl)oxy)hexyl)thioureido)benzoic acid TEA (GalH-FITC, 8)

A mixture of compound **7** (200.0 mg, 0.45 mmol) and FITC (174.0 mg, 0.45 mmol) were dissolved in anhydrous methanol (9 mL) containing triethylamine (63 μL, 0.45 mmol) and stirred in the dark for 24 h at ambient temperature. The result solution was evaporated, re-dissolved in dichloromethane and purified by silica gel chromatography (eluent, dichloromethane/2-propanol = 5/1). The crude product re-dissolved in methanol (25 mL) was treated with 0.5 M sodium methoxide in methanol (132 μL) at room temperature for 24 h to achieve deacetylation. The reaction solution was evaporated under vacuum to afford compound **8** (GalH-Gal) as a red solid (42.5 mg, 14% yield). ^{1}H NMR (400 MHz, methanol-d_4): δ 7.98 (s, 1H, H-15), 7.71 (d, J = 8.0 Hz, 1H, H-24), 7.19 (d, J = 8.0 Hz, 1H, H-26), 7.14–7.12 (m, 2H, H-9, H-27), 6.62–6.59 (m, 4H, H-16, H-18, H-21, H-23), 4.21 (d, J = 8.0 Hz, 1H, H-1′), 3.91 (dt, J = 9.6, 6.8 Hz, 1H, H-1), 3.82 (d, J = 2.4 Hz, 1H, H-4′), 3.75–3.70 (m, 2H, H-6′), 3.62–3.51 (m, 6H, H-2′, H-3′, H-5′, H-6, H-1), 3.01 (q, J = 7.6 Hz, 6H, CH_2), 1.71–1.32 (m, 8H, H-2, H-3, H-4, H-5), 1.16 (t, J = 7.6 Hz, 9H, CH_3); ^{13}C NMR (100 MHz, methanol-d_4): 182.1 (C, C═S, C-7), 176.6, 173.0 (C, C═O, C-11, C17, C22), 158.9 (C, C-8, C-10), 132.4 (CH, C-9, C2–7), 130.6 (CH, C-26), 126.3 (CH, C-15), 124.6 (CH, C-24), 121.6 (C, C-12, C-13), 114.6 (C, C-14, C-19, C-20, C25), 105.0 (CH, C-1′), 104.1 (C, C-16, C-18, C-21, C23), 76.6 (CH, C-5′), 75.0 (CH, C-3′), 72.6 (CH_2, C-3′), 70.7 (CH, C-1), 70.3 (CH, C-4′), 62.5 (CH_2, C-6′), 47.4 (CH_2), 40.6 (CH_2, C-6), 30.7, 29.9, 27.8, 26.8 (CH_2, C-2, C-5, C-3, C-4), 9.2 (CH_3); HRESI-MS: calcd for $C_{33}H_{37}N_2O_{11}S$ 669.2113 (M+1), found 669.2191 (MH^+).

2.2. Synthesis of ^{18}F-FBHGal (4b)

Compound **7** was conjugated with *N*-succinimidyl-4-^{18}F-fluorobenzoate (^{18}F-SFB) to afford the title compound ^{18}F-FBHGal. ^{18}F-SFB was synthesized from *tert*-butyl 4-*N*,*N*,*N*-trimethylammonium benzoate triflate (Sigma–Aldrich) as previously reported with minor modifications following the literature method.[27,28] The overall radiochemical yield of ^{18}F-SFB was about 40% (decay corrected, EOB) and the radiochemical purity was >95% determined using TLC method (silica gel $60F_{254}$ on an aluminum sheet, dichloromethane as the developing agent, R_f = 0.69). The purified ^{18}F-SFB was added to a acetonitrile solution containing compound **7** (300 μg) and *N*,*N*-diisopropylethylamine (20 μL). The reaction mixture was incubated at 50 °C for 30 min and hydrolyzed with sodium methoxide (1 M solution in methanol, 20 μL) at 60 °C for 15 min. After dilution with 1 mL of 0.1% acetic acid solution, the mixture was purified by semi-preparative HPLC system (Purospher® STAR RP-18, 5 μm, 250 mm × 10 mm, Merck, Darmstadt, Germany). A mixed solvent of acetonitrile and 0.1% acetic acid buffer (1/3, vol/vol) was used as the mobile phase (flow rate, 3 mL/min, ^{18}F-FBHGal retention time 10.5 min). The desired fraction was collected, evaporated to dryness, re-dissolved in normal saline and filtered through a 0.22 μm membrane filter (Millex-OR, Millipore) into a sterile vial to afford the final product of ^{18}F-FBHGal (**4b**) injection. The final product was identified by co-injection of an aliquot of product solution with authentic FBHGal (**4a**) using an analytical HPLC system (Purospher® STAR RP-18, 5 μm, 250 mm × 4 mm, Merck, Darmstadt, Germany; mobile phase: acetonitrile/0.1% acetic acid buffer = 1/3 (vol/vol); flow rate 0.8 mL/min). The stability of ^{18}F-FBHGal injection was determined by HPLC after storage at room temperature for 3 h.

2.3. ASGP receptor linked to uptake of GalH-FITC

Recombinant mouse ASGPR-1 (R&D Systems, Inc., Minneapolis) were coated (250, 500, 750 and 1500 ng/well) in 96 well plates. Sixteen hours later, an excess of FITC-conjugated galactose derivative (GalH-FITC, 250 ng/well) was added in the plates and incubated for 1 h at 37 °C. After extensive wash with PBS, fluorescence was counted in a TECAN Magellan microplate reader with an excitation wavelength of 495 nm and an emission wavelength of 521 nm.

2.4. Imaging of receptor-mediated endocytosis by confocal microscopy

The specific binding of galactose derivative to ASGP receptor was examined on HepG2 hepatocellular carcinoma cells which expressed high levels of ASGPR.[29] One day before the experiments, HepG2 cells were seeded at a density of 2×10^5 cells/well into 6-well plates containing collagen-coated glass coverslips. The cells were incubated with GalH-FITC (0.1 mL, 100 μM) in serum free MEM (0.9 mL) on ice for 1.5 h in the dark. After the binding step, the cells were washed extensively with cold PBS. Then fresh, prewarmed, MEM containing 10% fetal bovine serum was administered, and the cells were incubated at 37 °C for 30 min in a humidified CO_2 atmosphere (5%, v/v), leading to the internalization of the receptor-bound compounds into the cells. After the internalization step, the cells were washed twice with PBS and then fixed with 4% paraformaldehyde in PBS for 10 min at room temperature. After fixation, the coverslips were washed abundantly with PBS and mounted upside down. For blocking experiments, cells were incubated with asialofetuin (ASF, purchased from Sigma–Aldrich, 0.5 mg) for 30 min prior to incubation with GalH-FITC. Images of fixed cells were acquired on an Olympus FV-1000 laser scanning confocal system (FluoView FV1000; Olympus, Tokyo, Japan) with objective UPLSAPO 60× O NA: 1.35. Mean fluorescent intensity was evaluated with the ImageJ program.

2.5. Establishment of hepatic fibrosis in mouse

All experimental protocols involving animals were reviewed and approved by the institutional animal experimentation committee of the National Yang-Ming University. Male C57BL/6 mice (weighing 20–25 g, 8-weeks-old) were purchased from the National Laboratory Animal Center, Taiwan.

Hepatic fibrosis was induced using dimethylnitrosamine (DMN) following the literature method.[30,31] DMN (5 mg/mL in normal saline) at a dose of 10 mg/kg body weight was administered intraperitoneally on three consecutive days a week for 4 weeks. The sham group was injected with an equivalent amount of 0.9% normal saline with the same frequency. To validate the hepatic fibrosis, mice were sacrificed at 4 weeks after treated with DMN. The liver tissues were fixed with 4% phosphate-buffered paraformaldehyde and embedded in paraffin for Masson's trichrome staining.

2.6. Measurement of ASGPR protein content

The frozen liver tissue pieces (about 100 mg) of normal and hepatic fibrosis mice were homogenized in 0.25 M sucrose containing protease inhibitors (Complete Mini, Roche, Indianapolis, Indiana, USA), and the concentration of protein were determined using the Bio-Rad Protein Assay (Bio-Rad Laboratories, Hercules, CA, USA). An aliquot of homogenized suspension (containing 700 μg protein) was incubated with mouse ASGPR-1 primary antibody (polyclonal goat IgG, AF2755, R&D Systems, Minneapolis, MN, USA) for 2 h at 4 °C, then 30 μL of Protein A/G PLUS-Agarose (Santa Cruz Biotechnology, Santa Cruz, CA, USA) was added. After overnight incubation, beads were washed five times (500 μL lysis buffer each), and centrifuged at 2000*g* for 5 min. Proteins were eluted by adding 50 μL sample buffer and heating at 100 °C for 10 min. The samples were electrophoresed in a 10% SDS–polyacrylamide gel under reducing conditions and then transferred onto a polyvinylidene fluoride membrane (Perkin–Elmer Life Sciences, Boston, MA, USA). After blocking in 4% low-fat milk, the membrane was incubated sequentially with the mouse ASGPR-1 primary antibody (1:2000) followed by three times wash with PBS-T (PBS containing 0.05% Tween 20) and again incubated at room temperature for 2 h with horseradish peroxidase-conjugated anti-goat IgG secondary antibody (1:4000, Sigma, A5420, St. Louis, MO, USA). After incubation, the membrane was washed with PBS-T for five times and visualized by enhanced chemiluminescence detection according to the manufacturer's instructions (T-Pro Biotechnology, Taipei, Taiwan). The images were detected using LAS-4000 mini image analyzer system (Fujifilm, Tokyo, Japan).

2.7. In vivo biodistribution studies

In vivo biodistribution study was carried out in normal mice and hepatic fibrosis mice after intravenous injection of ^{18}F-FBHGal (3.7 MBq in 100 μL normal saline). At designated time points (5 and 30 min), mice (n = 4 at each time point) were sacrificed. The tissues and organs of interest were collected, wet weighed and assayed for radioactivity with a gamma counter (Wallac 1470 WIZARD Automatic Gamma Counter, Perkin–Elmer Life Science, Boston, MA, USA). The uptake of ^{18}F-FBHGal in tissues was expressed in counts per minute (cpm) corrected with decay and normalized to the percentage injected dose per gram of tissue (%ID/g). The receptor index was calculated by dividing the radioactivity of liver by that of liver plus heart 30 min post-injection (p.i.).

2.8. Metabolites analysis

Urine samples (100 μL) collected from normal mice at 30 min after a bolus injection of ^{18}F-FBHGal (7.4 MBq) were passed through a 0.45 μm nylon membrane filter (Pall Gelmann Laboratory, Ann Arbor, MI, USA). The radioactive components in the filtrate were assayed using the above-mentioned analytical HPLC system. The authentic compounds of possible metabolites, such as 4-fluoro-*N*-(6-hydroxyhexyl)-benzamide (FHB), 4-fluorobenzoic acid (FBA) and *N*-succinimidyl-4-fluorobenzoate (SFB) were purchased form Aldrich (Sigma–Aldrich, Germany) or synthesized and identified using nuclear magnetic resonance. The retention time of authentic FBHGal, FHB, FBA and SFB was about 8.7, 14.0, 17.9 and 23.5 min, respectively.

2.9. MicroPET imaging and pharmacokinetic studies

The microPET imaging was performed on a microPET R4 scanner (Concorde Microsystems, Inc., Knoxville, TN, USA) on Day 0, Day14 and Day 28 after treatment with DMN. The mice were anesthetized with 1% isoflurane in oxygen. Dynamic imaging was conducted to each group of mice (4 mice per group) for 60 min after intravenous injection of 7.4 ± 0.2 MBq of ^{18}F-FBHGal. Time–activity curves of heart and liver were generated from regions of interest (ROIs). The receptor index was derived by dividing the radioactivity of liver ROI by that of liver-plus-heart ROIs 30 min p.i. The pharmacokinetic parameters, including half-life ($T_{1/2}\alpha$ and $T_{1/2}\beta$), maximum blood concentrations (C_{max}), blood clearance (Cl), and areas under curves (AUCs), were estimated after fitting a nonlinear regression curve to the mean of heart radioactivity at each time point using the WinNonlin software (version 5.3; Pharsight Corp., Mountain View, CA, USA). Two-compartmental analysis (model, 7; input, iv-bolus) was used with the log/linear trapezoidal rule.

3. Results

3.1. Chemistry and radiochemistry

Starting from D-galactose, the β-D-galactosyl precursor (**7**) suitable for ^{18}F labeling can be obtained via a four-step synthesis with an overall yield of 25% (Fig. 1). The authentic FBHGal (**4a**) was prepared similarly with an overall yield of 22%. All reaction products were characterized by ^{1}H NMR, ^{13}C NMR and ESI-MS analysis. After coupling the precursor (**7**) with ^{18}F-SFB, ^{18}F-FBHGal (**4b**) was obtained with a high radiochemical purity (>98%, Fig. 2). The specific activity was 0.23 GBq/μmol as determined with HPLC using the standard addition method. The radiochemical yield of ^{18}F-FBHGal (decay corrected, EOB) was 20–25% after about 10 runs. The in vitro stability of ^{18}F-FBHGal in physiological saline at ambient temperature was good, the radiochemical purity was >98% after 3 h incubation (Fig. 2).

3.2. Establishment of hepatic fibrosis in mouse

After intermittent intraperitoneal injections (3 doses per week) of a small amount of DMN to mice for 4 weeks, histological liver examinations showed progressive deposition of collagen fiber in the liver (Fig. 3A). The liver parenchyma was uniformly divided into fibrotic nodules by fibrous septa. The results revealed extensive fibrosis accompanied with significant hepatocyte damage in the livers of DMN-treated mice. Although treatment-related body weight loss was noticed in fibrosis mice (Fig. 3B), the body weight change was less than 10% after 4-week DMN treatment.

3.3. ASGP receptor linked to uptake of GalH-FITC

To demonstrate the correlations between the fluorescent probe GalH-FITC and the target receptor ASGPR, we incubated GalH-FITC with different amounts of ASGPR and the data were calculated using a linear regression (Fig. 4A). High linear correlations between the amount of coated ASGPR and the retention of GalH-FITC in the wells were observed (r^2 = 0.99, P <0.01), suggested that the accumulation of monomeric galactose derivatives (either GalH-FITC or ^{18}F-FBHGal) may provide appropriate estimation of ASGPR expression level.

3.4. Imaging receptor-mediated endocytosis by confocal microscopy

HepG2 cells were incubated with GalH-FITC for 1.5 h on ice to allow binding to the receptors on cell membrane. In the washing step, unbound ligand was removed, and the cells were incubated for an additional 30 min at 37 °C to allow receptor-mediated endocytosis of bound ligand. Significant green fluorescence emission in the cytoplasm revealed receptor-mediated accumulation of GalH-FITC in HepG2 cells. Fluorescence was not observed in the nuclei (Fig. 4B).

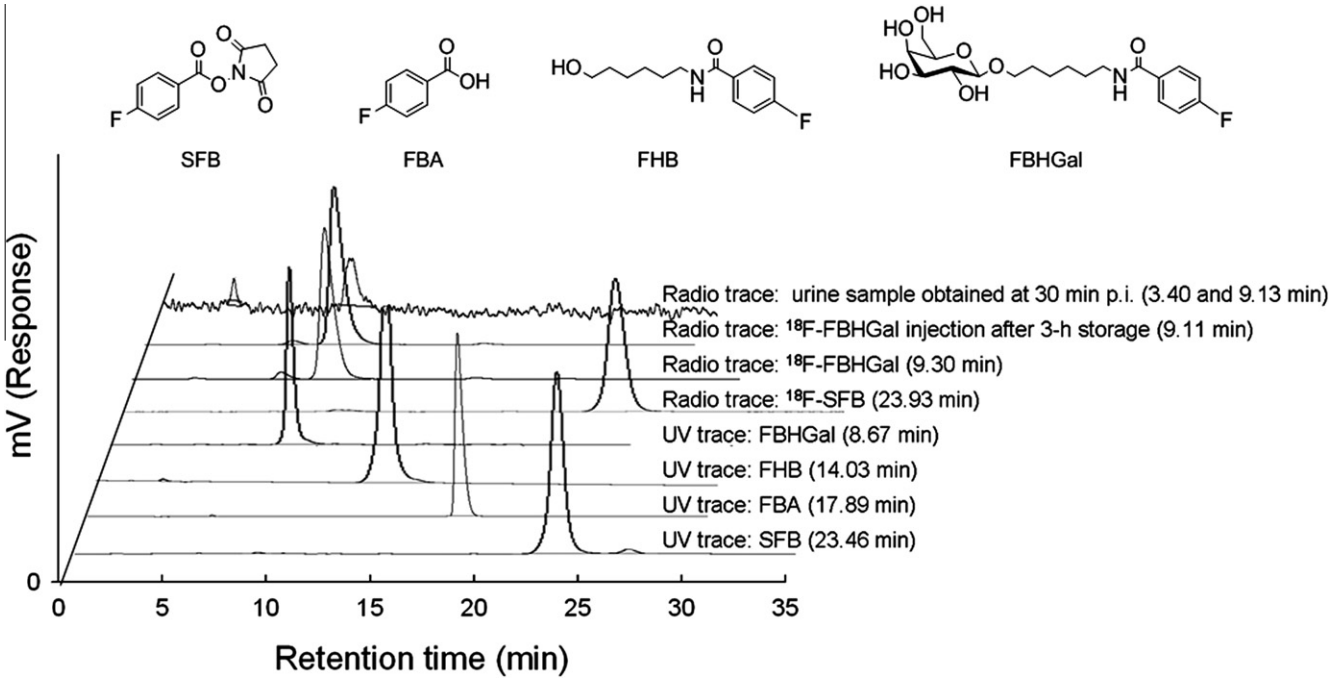

Figure 2. HPLC chromatograms of authentic FBHGal and some possible metabolites (FBA, SFB and FHB). Assay of radioactive components in ^{18}F-FBHGal injection (after 3-h storage) and in urine sample (obtained at 30 min p.i.) revealed the in vitro and in vivo stability of ^{18}F-FBHGal.

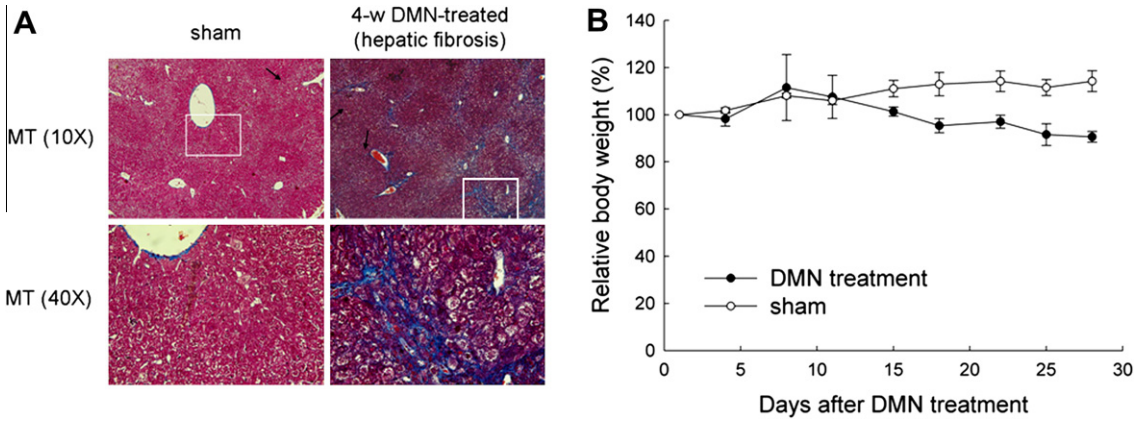

Figure 3. Effect of intraperitoneal injection of DMN (10 mg/kg of body weight) on liver histology and body weight change of the hepatic fibrosis mouse model. (A) Histological examination of liver tissues. After 4-week DMN or saline treatment (sham group), liver tissues were dissected, fixed, stained with Masson's trichrome (MT) and examined. Lower photographs show higher original magnification (40×) of respective upper photographs (10×). Arrows indicate fibrosis region. (B) The body weight loss during 12 doses of DMN and saline in C57B/L6 mice.

Asialofetuin (ASF), a natural glycoprotein having triantennary galactose terminal sugar chains, is known as an excellent ligand molecule selectively recognized by ASGPR. In the control group, ASF was added to saturate the binding site of ASGPR during the uptake period. The subcellular localization of GalH-FITC was largely reduced when co-incubated with a blocking dose of ASF (Fig. 4B). After incubation with GalH-FITC for 30 min, the average green fluorescence emission per HepG2 cell was about 7.1-fold (48.3 vs 6.82, P <0.0001) higher than those co-incubated with an equimolar concentration of ASF (Fig. 4C).

3.5. Measurement of ASGPR protein content

For human, the expression level of ASGPR was declined and the distribution was abnormal in cirrhosis liver.[13,32] Sawamura et al. reported that the density of ASGPR in liver could be largely reduced (maybe up to 70% reduction) in patients depends on the severity of liver cirrhosis.[13,14] In this study, the densitometric analysis of the immunoblots showed that ASGPR content in the liver of hepatic fibrosis mouse was decreased by an average of 23% compared with that of normal mouse (Fig. 5A). The results revealed that administration of DMN not only induce hepatic fibrosis, but also reduce the ASGPR expression in liver.

3.6. In vivo biodistribution

The biodistribution studies of ^{18}F-FBHGal were conducted in both normal and DMN-induced hepatic fibrosis mouse models to evaluate the distribution pattern in vivo (Table 1). At 30 min p.i., the liver uptake was 20.50 ± 1.51 %ID/g in normal mice, while that in the DMN-induced hepatic fibrosis mice was significantly reduced (14.84 ± 1.10 %ID/g, P <0.01). The receptor index was 0.95 ± 0.003 in normal mice, also remarkably higher than that in hepatic fibrosis mice (0.89 ± 0.01, P <0.001). At 30 min after

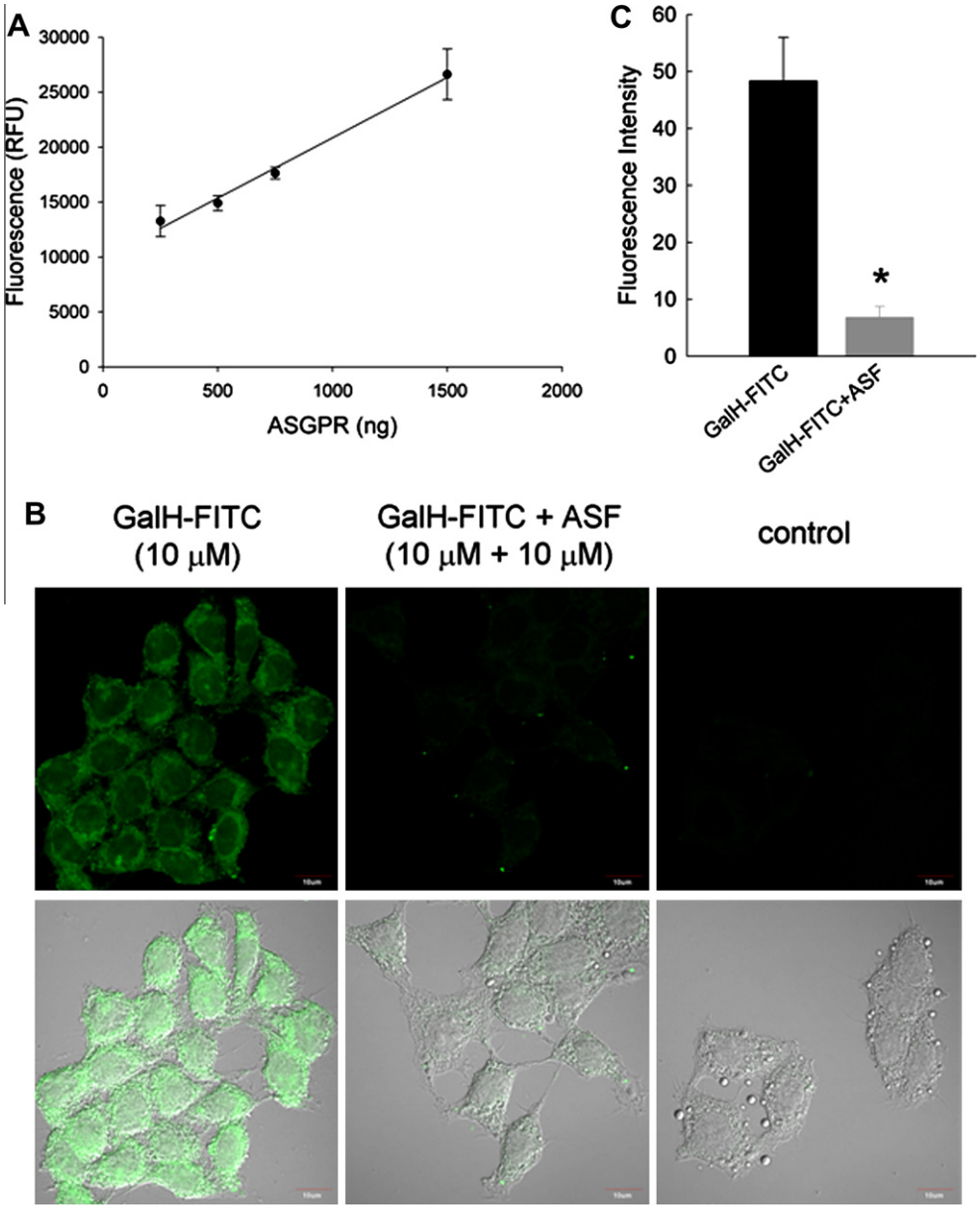

Figure 4. The selectivity and specificity of GalH-FITC to ASGPR in vitro. (A) Fluorescence emission from bound GalH-FITC was linearly proportional to the amount of coated ASGPR. (B) Confocal images of the HepG2 tumor cells after incubation with 10 μM of GalH-FITC with/without ASF. Significant green fluorescence emission in the cytoplasm revealed receptor-mediated accumulation of GalH-FITC in HepG2 cells. Fluorescence was not observed in the nuclei. In each picture, top is the fluorescence images and bottom is the optical merged images, respectively. Bars represent 10 μm. (C) Relative fluorescence intensity of GalH-FITC per cell derived from the confocal images shown in B. $^{*}P$ <0.01.

injection of ^{18}F-FBHGal in normal mice, high radioactivity collected in urine (1171.40 ± 269.07 %ID/g) suggested that excretion of ^{18}F-FBHGal was predominantly through the renal pathway. However, partial elimination via hepatobiliary system (43.89 ± 5.82 %ID/g in bile) was also observed. Less rapid blood clearance of ^{18}F-FBHGal in the hepatic fibrosis mice was noticed. The radioactivity retention in kidney and blood of the hepatic fibrosis mice (8.13 ± 1.19 %ID/g in kidney; 2.61 ± 0.37 %ID/g in blood) at 30 min p.i. was significantly higher than those of the normal mice (4.6 ± 0.92 %ID/g in kidney, P <0.01; 1.60 ± 0.24 %ID/g in blood, P <0.01).

3.7. Metabolites analysis

The radioactive metabolites in urine after administration of ^{18}F-FBHGal in normal mouse were assayed by HPLC (Fig. 2). Intact ^{18}F-FBHGal accounted for ~80% of radioactivity in the urine at 30 min p.i., indicated high in vivo stability in the mouse model. None of the above-mentioned possible radioactive metabolites, for example, FHB, FBA, SFB, were detected in the urine.

3.8. MicroPET imaging and pharmacokinetic studies

A 1-h dynamic microPET scan of normal mouse was conducted immediately after ^{18}F-FBHGal injection via the tail vein. The images revealed predominant hepatic uptake began soon after tracer injection, increased rapidly, reached plateau within 10 min and only slightly declined till 1 h p.i. The noted accumulation in kidney and bladder revealed that renal clearance is the predominant route of excretion. The nonspecific uptake in other organs was at very low level in normal mice. Representative coronal and transaxial

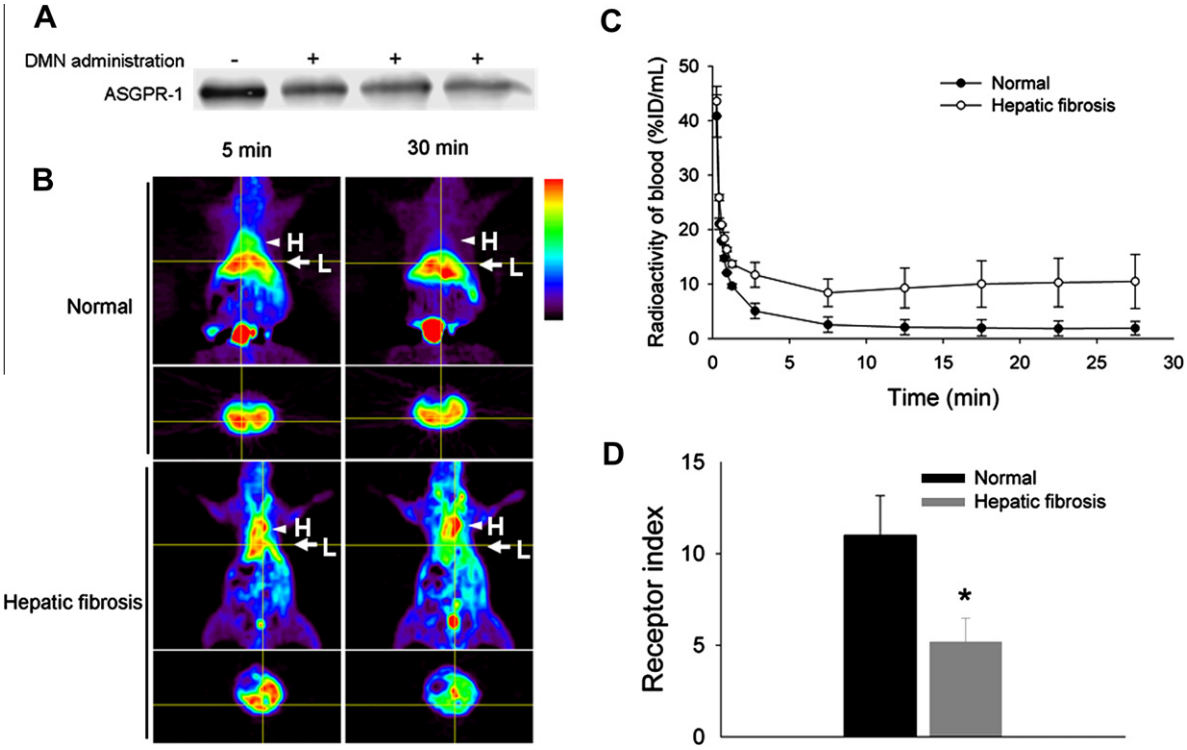

Figure 5. ^{18}F-FBHGal microPET imaging of normal and hepatic fibrosis mice. (A) Western blotting of ASGPR-1 in liver tissues. (B) Coronal (top) and transaxial (bottom) images of normal and hepatic fibrosis mice at 5 and 30 min after intravenous injection of ~3.7 MBq of ^{18}F-FBHGal; L, liver; H, heart. (C) Time–activity curves of ^{18}F-FBHGal in heart of normal mice and hepatic fibrosis mice derived from dynamic microPET images. (D) The receptor index derived from microPET images. (n = 4 per group; bars represent means ± SD). $^{*}P$ <0.01, compared with control mice group by student paired t test.

Table 1
Biodistribution of ^{18}F-FBHGal in normal and hepatic fibrosis mice at 5 and 30 min after intravenous injection of 3.7 MBq of ^{18}F-FBHGal

	Normal mice		Induced liver fibrosis mice	
	5 min	30 min	5 min	30 min
Blood	3.82 ± 0.69*	1.60 ± 0.24*	5.83 ± 0.50*	2.61 ± 0.37*
Heart	1.53 ± 0.06*	1.14 ± 0.05*	2.42 ± 0.12*	1.73 ± 0.11*
Lung	1.83 ± 0.40*	0.83 ± 0.20	3.32 ± 0.29*	1.12 ± 0.22
Stomach	2.50 ± 0.87	0.88 ± 0.05	2.83 ± 0.29	1.50 ± 0.57
SI	5.01 ± 0.11*	2.86 ± 0.24	7.86 ± 1.03*	3.18 ± 1.33
LI	2.04 ± 0.32	0.90 ± 0.12	2.90 ± 0.45	1.19 ± 0.22
Spleen	1.33 ± 0.07*	0.70 ± 0.15	2.17 ± 0.18*	0.75 ± 0.27
Pancreas	2.72 ± 0.18*	0.93 ± 0.10*	4.15 ± 0.38*	1.59 ± 0.30*
Muscle	0.95 ± 0.10*	0.66 ± 0.09*	1.54 ± 0.10*	1.00 ± 0.07*
Bone	0.96 ± 0.04	0.67 ± 0.08	1.32 ± 0.62	0.77 ± 0.13
Kidney	30.09 ± 7.95	4.66 ± 0.92*	32.67 ± 1.46	8.13 ± 1.19*
Bile	11.84 ± 0.52	43.89 ± 5.82	99.33 ± 92.10	37.14 ± 5.92
Urine	385.32 ± 289.12	1171.40 ± 269.07	425.56 ± 149.09	294.80 ± 127.68
Feces	0.76 ± 0.09	1.98 ± 0.69	1.16 ± 0.31	1.08 ± 0.32
Liver	24.39 ± 3.38	20.50 ± 1.51*	18.86 ± 2.85	14.84 ± 1.10*
RI		0.95 ± 0.003*		0.89 ± 0.01*

Expressed as percentage injection dose per gram of organ (%ID/g). Each value represents the mean ± SD (n = 4). SI, small intestine; LI, large intestine; RI, receptor index.
* Significant difference between control mice and hepatic fibrosis group, two-tailed t test, P <0.01.

microPET images of the normal and hepatic fibrosis mice at 5–10 and 25–30 min p.i. were shown in Figure 5B. The uptake levels of interested organs were quantitated by measuring ROIs encompassing the organ in the microPET coronal images. The receptor index was 0.74 ± 0.05 in normal mice, again appreciably higher than that in hepatic fibrosis mice (0.46 ± 0.09, n = 4 in each group, P = 0.004, Fig. 5D). The results of microPET imaging coincide with those observed in biodistribution studies.

The time–radioactivity curves of ^{18}F-FBHGal in normal and hepatic fibrosis mice were shown in Figure 5C. The pharmacokinetic parameters derived from these curves were summarized in Table 2. The radioactivity in blood declined in a bi-exponential way after injection of ^{18}F-FBHGal and the data fit well to a two-compartment pharmacokinetic model. Following intravenous administration of ^{18}F-FBHGal in normal mice, the time–radioactivity curve of blood exhibited a rapid distribution phase with a mean distribution half-life ($T_{1/2}\alpha$) of 0.09 min followed by a relatively slower elimination phase with a half-life ($T_{1/2}\beta$) of 1.48 min (Fig. 5C). The distribution and elimination half-lives of ^{18}F-FBHGal in hepatic fibrosis mice were much longer than those in normal mice (2.1- and 55.8-fold, respectively). The AUC of ^{18}F-FBHGal in blood of hepatic fibrosis mice were 1434.66 min %ID/mL, which is 23.9-fold higher than that in normal mice (60.15 min %ID/mL). The faster blood clearance (Cl) in normal mice may explain the lower AUC. The

Table 2
Estimated pharmacokinetic parameters derived from microPET images of mice after intravenous injection of ^{18}F-FBHGal

Parameter	Unit	Normal mice	Four-week DMN-treated mice
$T_{1/2}\alpha$	min	0.09	0.19
$T_{1/2}\beta$	min	1.48	82.55
C_{max}	%ID/mL	170.78	87.60
Cl	μCi/min × (%ID/mL)	1.16	0.05
AUC	min × %ID/mL	60.15	1434.66

Values were derived by data of mean (n = 4). Calculated with the WinNonlin program (for a two compartmental model). $T_{1/2}$, half-life; C_{max}, maximum radioactivity; Cl, blood clearance; AUC, area under the curve.

results revealed prolonged systemic circulation of ^{18}F-FBHGal in hepatic fibrosis mice compared to that in normal mice.

4. Discussion

Measurement of hepatic function in liver fibrosis patients has been linked to several complications, such as ascites, encephalopathy, and portal hypertension. Noninvasive quantification of the ASGPR density on the hepatocytes in vivo provided unambiguous evaluation of hepatic function. ^{99m}Tc-labeled galactosyl-neoglycoalbumin (^{99m}Tc-NGA) and galactosyl-human serum albumin (^{99m}Tc-GSA) have been used as ASGPR-binding agents in clinical studies. However, using albumin-based detection probe may debate on systemic changes that include cardiovascular, hematological, renal, pulmonary, and immunological effects.[33] In addition, those tracers using albumin backbone usually have high stability in the bloodstream and a long circulation time, which is unfavorable for a diagnostic probe. Positron emission tomography (PET) is one of the most sensitive molecular imaging techniques, and fluorine-18 has the most favorable physical properties in all the positron nuclides employed in PET. This study developed a new ^{18}F-labeled monomeric galactoside ^{18}F-FBHGal as an ASGPR probe for PET imaging. Biological characterization demonstrated that ^{18}F-FBHGal was promising for quantitative assay of ASGPR with fast pharmacokinetics in mouse models.

ASF, containing 12.4 galactose and 1.6 galactosamine moieties in one molecule, exhibited high binding capacity (14-fold higher than a GalH-FITC molecule) to ASGPR.[34] When co-incubated with an equimolar concentration of ASF, the uptake of GalH-FITC in HepG2 cells observed under confocal microscopy was almost completely blocked. The residual contrast in the blocking experiment is probably due to nonspecific accumulation in the extracellular space. A competitive binding assay was conducted to evaluate the binding affinity of nonradioactive FBHGal using ^{131}I-labeled ASF as a reference compound. FBHGal exhibited an IC_{50} value of 1.53 mM for the ASGPR on HepG2 cells (data not shown), similar to those of monovalent galactose derivatives reported in earlier literature.[35–37] The results of in vitro studies demonstrated that both GalH-FITC and ^{18}F-FBHGal displayed specific binding to ASGP receptor.

Both biodistribution studies and microPET imaging revealed high and sustained accumulation of ^{18}F-FBHGal in the liver of normal mice (24.39–20.50 %ID/g from 5 to 30 min p.i. in biodistribution studies). Noted radioactivity in kidneys and urine indicated that ^{18}F-FBHGal and its radioactive metabolites excreted primarily through the urinary system (Fig. 2). In other organs, except the kidneys, rapid clearance of ^{18}F-FBHGal was observed and the uptakes were less than 1.0 %ID/g at 30 min p.i. For the albumin-based probes, however, ^{18}F-labeled NGA[20] exhibited rather shorter liver retention, 79.18–13.85 %ID/g from 5 to 30 min p.i., while ^{99m}Tc-labeled neolactosyl human serum albumin (LSA)[38] and NGA[39] showed slower clearance (≧5 %ID/g) from several major organs, for example, spleen, stomach, intestine and bone, of normal mice.

Liver fibrosis in experimental animals can be produced by a variety of methods involving induction by hepatotoxic agents (e.g., dimethylnitrosamine (DMN),[30,31] carbon tetrachloride[40] and ethanol[41]), bile duct ligation[42] or using transgenic animals.[43,44] Of the methods that were currently employed, DMN-induced liver fibrosis in mouse is simple, relatively inexpensive, reproducible, and displays many of the features of human cirrhosis. The biodistribution of ^{18}F-FBHGal in liver, and also in many other organs, of healthy and hepatic fibrosis mice after intravenous injection was significantly different (Table 1). The liver uptake was higher in healthy than in fibrosis mice, while the remaining blood activity was higher in fibrosis mice than in healthy ones. Liver is a vital blood reservoir of body. The liver uptake derived from the liver ROI of microPET images may be overestimated due to the contribution of blood in it, especially in the cases of hepatic fibrosis mice. Receptor index has been reported as a useful diagnostic parameter in estimating the dysfunction of hepatocytes.[19,45,46] In this study, we demonstrated that receptor index derived from the microPET images is able to distinguish the fibrosis liver from the healthy (Fig. 5D). The time–radioactivity curves of blood derived from microPET images (Fig. 5C) were consistent with those observed in biodistribution studies.

Ablation of ASGPRs on the hepatocytes reported in the process of fibrosis[13,47] was also observed in this DMN-induced hepatic fibrosis mouse model (Fig. 5A). Steirer et al.[48] reported that ASGPR contributed to the regulation of the relative concentrations of plasma glycoproteins bearing terminal galactose. Due to the decrease of ASGPR, the increased amount of serum asialoglycoproteins as native ASGPR ligands might compete against the radiotracer with terminal galactose. Thus, after administration of ^{18}F-FBHGal in hepatic fibrosis mice, the uptake of tracer by the fibrosis liver through receptor-mediated process would be reduced and led to longer retention in blood by either coherent decrease of ASGPR or competition with the native ASGPR ligands. After binding to ligand, internalizing into the cell, and dissociating from its ligands within the acidic environment of the sorting compartment, ASGPR will recycle back to the cell surface within 8 min.[49] The remanent ASGPRs in hepatic fibrosis liver still function and reveal perceivably accumulation of ^{18}F-FBHGal. Moerover, the monovalent galactoside ^{18}F-FBHGal, with a relatively lower binding affinity than multivalent ligands, revealed a lower hepatic uptake (24.39 ± 3.38 %ID/g) than ^{18}F-FNGA (79.18 ± 7.17 %ID/g)[20] at 5 min post injection in normal mice. The differences in liver uptakes between normal and hepatic fibrosis mice, though not remarkable in ^{18}F-FBHGal PET imaging, still reached statistical significance in biodistribution study (P <0.01). Except liver, radioactivity accumulation in other organs such as heart, blood, lung, pancreas, kidney and muscle, were significant higher compared to those of normal mice mainly due to the higher remanent radioactivity in blood. Yang et al. have demonstrated in an inhibition study[20,39] that, most ASGP receptors on the hepatocyte membrane were occupied when excess inhibitor was preinjected, a condition similar to the hepatic cirrhosis in which the available receptors were largely reduced. For the patients suffering severe liver fibrosis or cirrhosis, administration of albumin-based ASGPR binding radiotracers, such as ^{18}F-FNGA and ^{99m}Tc-NGA that were currently used, would provide only vague liver images due to significant retention of radiotracers (in %ID/g) in bloodstream as well as in liver.[22,50] Compared with albumin- or polymer-based ligands,[22,50] ^{18}F-FBHGal can be rapidly excreted from blood and normal organs via the urinary system in its intact form (Fig. 2) in mice and thus the re-uptake of radiotracer by the recycled receptor would be limited.

5. Conclusion

In this study, an ASGPR-specific probe conjugated with FITC or labeled with fluorine-18 was developed and characterized with HepG2 hepatoma cells (high ASGPR expression) and a hepatic fibrosis mouse model. The in vitro studies demonstrated that GalH-FITC can be specifically bound and internalized into HepG2 cells through ASGP receptor-mediated endocytosis. ^{18}F-FBHGal, with its highly specific ASGPR-targeting ability, good in vivo stability, and the exhibition of significantly different pharmacokinetic properties in normal and DMN treated mice, is demonstrated a feasible PET probe for monitoring hepatic fibrosis in mice, and may provide new insights into the ASGPR-related liver diseases.

Acknowledgements

This study was supported by grants from the Institute of Nuclear Energy Research of Taiwan (982001INER071 and 992001INER081). We thank the staff of the Molecular and Genetic Imaging Core/National Research Program for Genomic Medicine (NSC100-2319-B010-003) who kindly provided the radioisotope and excellent technical assistance. The technical support in part by the Imaging Core Facility of Nanotechnology in National Yang-Ming University and the Division of Experiment Surgery of the Department of Surgery in Taipei Veterans General Hospital are also gratefully acknowledged.

Supplementary data

Supplementary data associated with this article can be found, in the online version, at http://dx.doi.org/10.1016/j.bmc.2012.12.022.

References and notes

1. Department of Health, E. Y., Taiwan. 2011. http://www.doh.gov.tw/ufile/doc/99%E5%B9%B4%E7%89%88%E5%85%AC%E5%85%B1%E8%A1%9B%E7%94%9F%E5%B9%B4%E5%A0%B1.pdf.
2. Bataller, R.; Brenner, D. A. *J. Clin. Invest.* **2005**, *115*, 209.
3. Levrero, M. *Oncogene* **2006**, *25*, 3834.
4. Benyon, R. C.; Iredale, J. P. *Gut* **2000**, *46*, 443.
5. Martinez, S. M.; Crespo, G.; Navasa, M.; Forns, X. *Hepatology* **2011**, *53*, 325.
6. Thabut, D.; Moreau, R.; Lebrec, D. *Hepatology* **2011**, *53*, 683.
7. Castera, L.; Forns, X.; Alberti, A. *J. Hepatol.* **2008**, *48*, 835.
8. Friedrich-Rust, M.; Wunder, K.; Kriener, S.; Sotoudeh, F.; Richter, S.; Bojunga, J.; Herrmann, E.; Poynard, T.; Dietrich, C. F.; Vermehren, J.; Zeuzem, S.; Sarrazin, C. *Radiology* **2009**, *252*, 595.
9. Ashwell, G.; Morell, A. G. *Adv. Enzymol. Relat. Areas Mol. Biol.* **1974**, *41*, 99.
10. Stokmaier, D.; Khorev, O.; Cutting, B.; Born, R.; Ricklin, D.; Ernst, T. O.; Boni, F.; Schwingruber, K.; Gentner, M.; Wittwer, M.; Spreafico, M.; Vedani, A.; Rabbani, S.; Schwardt, O.; Ernst, B. *Bioorg. Med. Chem.* **2009**, *17*, 7254.
11. Ashwell, G.; Harford, J. *Annu. Rev. Biochem.* **1982**, *51*, 531.
12. Stockert, R. J. *Physiol. Rev.* **1995**, *75*, 591.
13. Sawamura, T.; Nakada, H.; Hazama, H.; Shiozaki, Y.; Sameshima, Y.; Tashiro, Y. *Gastroenterology* **1984**, *87*, 1217.
14. Sawamura, T.; Kawasato, S.; Tsuda, M.; Naitoh, Y.; Shiozaki, Y.; Sameshima, Y. *Gastroenterol. Jpn.* **1985**, *20*, 201.
15. Vera, D. R.; Stadalnik, R. C.; Krohn, K. A. *J. Nucl. Med.* **1985**, *26*, 1157.
16. Stadalnik, R. C.; Vera, D. R.; Woodle, E. S.; Trudeau, W. L.; Porter, B. A.; Ward, R. E.; Krohn, K. A.; O'Grady, L. F. *J. Nucl. Med.* **1985**, *26*, 1233.
17. Matsuzaki, S.; Onda, M.; Tajiri, T.; Kim, D. Y. *Hepatology* **1997**, *25*, 828.
18. Ohno, Y.; Ishida, H.; Hayashi, A.; Kamagata, S.; Hirobe, S.; Ishii, K. *J. Nucl. Med.* **2002**, *43*, 1611.
19. Sasaki, N.; Shiomi, S.; Iwata, Y.; Nishiguchi, S.; Kuroki, T.; Kawabe, J.; Ochi, H. *J. Nucl. Med.* **1999**, *40*, 1652.
20. Yang, W.; Mou, T.; Peng, C.; Wu, Z.; Zhang, X.; Li, F.; Ma, Y. *Bioorg. Med. Chem.* **2009**, *17*, 7510.
21. Kim, E. M.; Jeong, H. J.; Park, I. K.; Cho, C. S.; Kim, C. G.; Bom, H. S. *J. Nucl. Med.* **2005**, *46*, 141.
22. Yang, W.; Mou, T.; Shao, G.; Wang, F.; Zhang, X.; Liu, B. *J. Nucl. Med.* **2011**, *52*, 978.
23. Sawamura, T.; Kawasato, S.; Shiozaki, Y.; Sameshima, Y.; Nakada, H.; Tashiro, Y. *Gastroenterology* **1981**, *81*, 527.
24. Woodle, E. S.; Vera, D. R.; Stadalnik, R. C.; Ward, R. E. *Surgery* **1987**, *102*, 55.
25. Baenziger, J. U.; Maynard, Y. *J. Biol. Chem.* **1980**, *255*, 4607.
26. Kim, S. H.; Goto, M.; Akaike, T. *J. Biol. Chem.* **2001**, *276*, 35312.
27. Okarvi, S. M. *Eur. J. Nucl. Med.* **2001**, *28*, 929.
28. Chuang, C. H.; Chuang, K. H.; Wang, H. E.; Roffler, S. R.; Shiea, J. T.; Tzou, S. C.; Cheng, T. C.; Kao, C. H.; Wu, S. Y.; Tseng, W. L.; Cheng, C. M.; Hou, M. F.; Wang, J. M.; Cheng, T. L. *Clin. Cancer Res.* **2012**, *18*, 238.
29. Schwartz, A. L.; Fridovich, S. E.; Knowles, B. B.; Lodish, H. F. *J. Biol. Chem.* **1981**, *256*, 8878.
30. Jang, J. H.; Kang, K. J.; Kim, Y. H.; Kang, Y. N.; Lee, I. S. *Transplant. Proc.* **2008**, *40*, 2700.
31. Ogata, H.; Chinen, T.; Yoshida, T.; Kinjyo, I.; Takaesu, G.; Shiraishi, H.; Iida, M.; Kobayashi, T.; Yoshimura, A. *Oncogene* **2006**, *25*, 2520.
32. Hilgard, P.; Schreiter, T.; Stockert, R. J.; Gerken, G.; Treichel, U. *Hepatology* **2004**, *39*, 1398.
33. Pulimood, T. B.; Park, G. R. *Crit. Care* **2000**, *4*, 151.
34. Spiro, R. G. *J. Biol. Chem.* **1960**, *235*, 2860.
35. Collins, B. E.; Paulson, J. C. *Curr. Opin. Chem. Biol.* **2004**, *8*, 617.
36. Groman, E. V.; Enriquez, P. M.; Jung, C.; Josephson, L. *Bioconjugate Chem.* **1994**, *5*, 547.
37. Schwartz, A. L. *CRC Crit. Rev. Biochem.* **1984**, *16*, 207.
38. Jeong, J. M.; Hong, M. K.; Lee, J.; Son, M.; So, Y.; Lee, D. S.; Chung, J. K.; Lee, M. C. *Bioconjugate Chem.* **2004**, *15*, 850.
39. Yang, W.; Mou, T.; Zhang, X.; Wang, X. *Appl. Radiat. Isot.* **2010**, *68*, 105.
40. Louis, H.; Van Laethem, J. L.; Wu, W.; Quertinmont, E.; Degraef, C.; Van den Berg, K.; Demols, A.; Goldman, M.; Le Moine, O.; Geerts, A.; Deviere, J. *Hepatology* **1998**, *28*, 1607.
41. Barak, A. J.; Beckenhauer, H. C.; Kerrigan, F. J. *Gut* **1967**, *8*, 454.
42. Ebrahimkhani, M. R.; Kiani, S.; Oakley, F.; Kendall, T.; Shariftabrizi, A.; Tavangar, S. M.; Moezi, L.; Payabvash, S.; Karoon, A.; Hoseininik, H.; Mann, D. A.; Moore, K. P.; Mani, A. R.; Dehpour, A. R. *Gut* **2006**, *55*, 1606.
43. Paradis, V.; Dargere, D.; Vidaud, M.; De Gouville, A. C.; Huet, S.; Martinez, V.; Gauthier, J. M.; Ba, N.; Sobesky, R.; Ratziu, V.; Bedossa, P. *Hepatology* **1999**, *30*, 968.
44. Kanzler, S.; Lohse, A. W.; Keil, A.; Henninger, J.; Dienes, H. P.; Schirmacher, P.; Rose-John, S.; Zum Buschenfelde, K. H.; Blessing, M. *Am. J. Physiol.* **1999**, *276*, G1059.
45. Kudo, M.; Todo, A.; Ikekubo, K.; Hino, M. *Am. J. Gastroenterol.* **1992**, *87*, 865.
46. Shiomi, S.; Sasaki, N.; Tamori, A.; Habu, D.; Takeda, T.; Nishiguchi, S.; Kuroki, T.; Kawabe, J.; Ochi, H. *J. Gastroenterol. Hepatol.* **1999**, *14*, 566.
47. Burgess, J. B.; Baenziger, J. U.; Brown, W. R. *Hepatology* **1992**, *15*, 702.
48. Steirer, L. M.; Park, E. I.; Townsend, R. R.; Baenziger, J. U. *J. Biol. Chem.* **2009**, *284*, 3777.
49. Schwartz, A. L.; Ciechanover, A.; Merritt, S.; Turkewitz, A. *J. Biol. Chem.* **1986**, *261*, 15225.
50. Yang, W.; Mou, T.; Guo, W.; Jing, H.; Peng, C.; Zhang, X.; Ma, Y.; Liu, B. *Bioorg. Med. Chem. Lett.* **2010**, *20*, 4840.